Potential of X-Band TerraSAR-X and COSMO-SkyMed SAR Data for the Assessment of Physical Soil Parameters

Azza Gorrab, Mehrez Zribi, N. Baghdadi, Bernard Mougenot, Z. Lili Chabaane

Remote Sens. **2015**, *7*, 747-766; doi:10.3390/rs70100747

OPEN ACCESS

remote sensing

ISSN 2072-4292

www.mdpi.com/journal/remotesensing

Article

Potential of X-Band TerraSAR-X and COSMO-SkyMed SAR Data for the Assessment of Physical Soil Parameters

Azza Gorrab [1,2,*], Mehrez Zribi [1], Nicolas Baghdadi [3], Bernard Mougenot [1] and Zohra Lili Chabaane [2]

[1] CESBIO (CNRS/UPS/IRD/CNES), 18 av. Edouard Belin, 31401 Toulouse Cedex 9, France; E-Mails: mehrez.zribi@cesbio.cnes.fr (M.Z.); bernard.mougenot@ird.fr (B.M.)

[2] University of Carthage/INAT, 43 av. Charles Nicolle 1082, Tunis, Mahrajène Tunisie, Tunisia; E-Mail: zohra.lili.chabaane@gmail.com

[3] IRSTEA, UMR TETIS, 500 rue François Breton, 34093 Montpellier Cedex 5, France; E-Mail: nicolas.baghdadi@teledetection.fr

* Author to whom correspondence should be addressed; E-Mail: azzagorrab@gmail.com; Tel.: +33-561-558-525.

Academic Editor: Yoshio Inoue and Prasad S. Thenkabail

Received: 10 September 2014 / Accepted: 6 January 2015 / Published: 12 January 2015

Abstract: The aim of this paper is to analyze the potential of X-band SAR measurements (COSMO-SkyMed and TerraSAR-X) made over bare soils for the estimation of soil moisture and surface geometry parameters at a semi-arid site in Tunisia (North Africa). Radar signals acquired with different configurations (*HH* and *VV* polarizations, incidence angles of 26° and 36°) are statistically compared with ground measurements (soil moisture and roughness parameters). The radar measurements are found to be highly sensitive to the various soil parameters of interest. A linear relationship is determined for the radar signals as a function of volumetric soil moisture, and a logarithmic correlation is observed between the radar signals and three surface roughness parameters: the root mean square height (Hrms), the parameter $Zs = Hrms^2/l$ (where l is the correlation length) and the parameter $Zg = Hrms \times (Hrms/l)^{\alpha}$ (where α is the power of the surface height correlation function). The highest dynamic sensitivity is observed for *Zg* at high incidence angles. Finally, the performance of different physical and semi-empirical backscattering models (IEM, Baghdadi-calibrated IEM and Dubois models) is compared with SAR measurements. The results provide an indication of the limits of validity of the IEM and Dubois models, for various radar configurations and roughness conditions. Considerable improvements in

the IEM model performance are observed using the Baghdadi-calibrated version of this model.

Keywords: soil moisture; soil roughness; TerraSAR-X; COSMO-SkyMed; SAR; IEM; Baghdadi-calibrated IEM model; Dubois model

1. Introduction

Physical soil properties such as roughness and moisture need to be estimated in various scientific applications, such as hydrological and erosion modeling, agriculture, and the management of sustainable natural resources [1,2]. The parameters characterizing agricultural soils have very high spatial and temporal variabilities, and conventional spot soil moisture and surface roughness measurements do not provide an adequate description of this variability. Imaging Synthetic Aperture Radar (SAR) sensors have demonstrated their potential to effectively measure and monitor soil surface characteristics at a high spatial resolution [3–9]. Over bare agricultural areas, the backscattered radar signal is very sensitive to dielectric (soil moisture) and geometric (roughness) soil surface properties [10–12]. Consequently, different radar backscattering models (physical, semi-empirical, and empirical) have been developed to improve scientific understanding of the relationship between the backscattering coefficient and the parameters used to characterize the soil. The most frequently used models are the Integral Equation Model IEM of Fung *et al.* [13,14] and the Advanced Integrated Equation Model (AIEM) [15,16], which are applicable to a large range of soil roughness conditions, as well as semi-empirical models such those of Oh [17] and Dubois [18], which provide simple analytical relationships between the backscattered radar signal and physical soil parameters.

In recent years, various improvements have been achieved in the performance of existing backscattering models [19–21], in particular by enlarging their field of applicability. Various studies have contributed to the use of a more complete description of soil surface roughness for forward studies [22–30]. Zribi *et al.* [26] introduced fractal and Brownian approaches to describe the correlation function, whereas Li *et al.* [20] proposed a general power law description of roughness spectra. Fung [14] proposed different types of analytical correlation function, used to fit the experimental data.

In addition, other studies have been proposed to improve the description of surface parameters in contexts where the measurements are achieved with only a small number of radar data configurations and the resulting need to retrieve only a small number of surface parameters. Zribi and Dechambre [31] proposed the introduction of a new parameter, Zs, equal to $Hrms^2/l$, which combines the effects of two roughness descriptions (rms height and correlation length) in one single parameter, and Zribi *et al.* [32] proposed a global parameter combining the influence of three conventional parameters (rms height, height correlation length, and correlation function shape). Lievens *et al.* [30] showed that roughness parameters can vary from one SAR acquisition to another, since they are related to the observed backscatter coefficients, and to variations in local incidence angle. A statistical model was thus developed to estimate effective roughness parameters from radar observations. Baghdadi *et al.* [33–36] define a new empirical correlation length, Lopt, calculated as a function of the rms surface height and

the characteristics of the remote sensing radar (frequency, incidence angle and polarization), allowing an improved fit to be achieved between IEM simulations and radar observations.

Despite these contributions, the influence of roughness is still poorly modelled in currently known inversion techniques, and most of these studies were made in the C band. Only a small number of studies have discussed the potential applications of X-band data [11,12,37].

In this context, the aim of the present paper is to analyze the behavior of X-band radar data acquired with the TerraSAR-X and COSMO-SkyMed sensors as a function of physical soil parameters (moisture and roughness), and to compare these results with the predictions of the most commonly used backscattering models. Section 2 describes the study site, satellite images and ground measurement database. Section 3 provides a statistical analysis of the relationships established between backscattered radar signals and soil parameters. Section 4 compares the performance of the different backscattering models. Our conclusions are provided in Section 5.

2. Study Site and Database Description

2.1. Study Site Description

Our study site is situated in the Kairouan plain (9°23′−10°17′E, 35°1′−35°55′N (Figure 1)), in central Tunisia. The climate in this region is semi-arid, with an average annual rainfall of approximately 300 mm/year, characterized by a rainy season lasting from October to May, with the two rainiest months being October and March [9]. As is generally the case in semi-arid areas, the rainfall patterns in this area are highly variable in time and space. The mean temperature in Kairouan City is 19.2 °C (minimum of 10.7 °C in January and maximum of 28.6 °C in August). The mean annual potential evapotranspiration (Penman) is close to 1600 mm. The landscape is mainly flat, and the vegetation is dominated by agricultural production (cereals, olive groves, fruit trees, market gardens and bare soils).

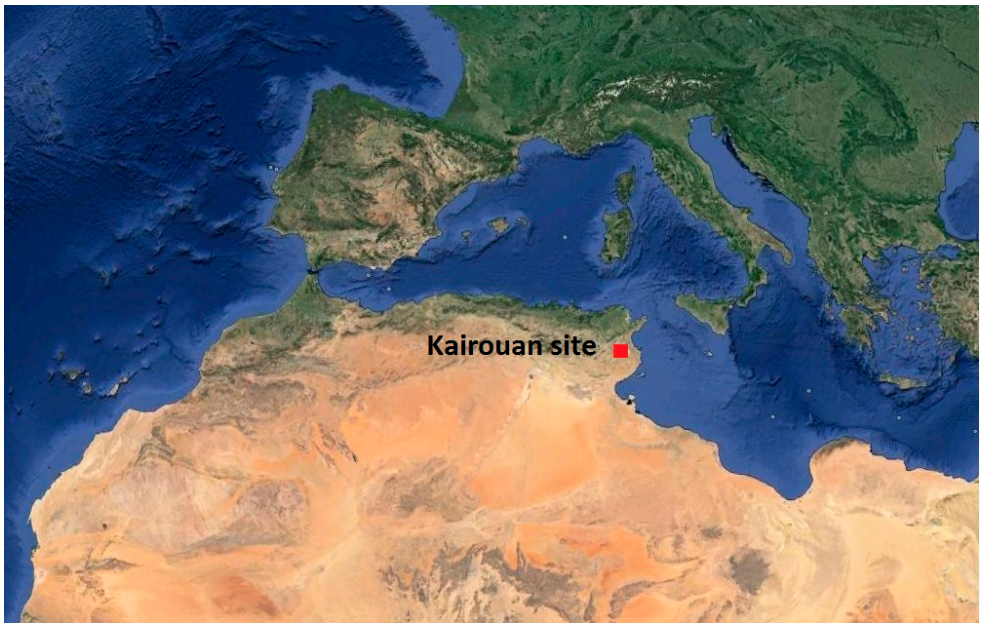

Figure 1. Location of the study site.

2.2. Database Description

2.2.1. Satellite Images

Eleven radar images (X-Band ~ 9.65 GHz) were acquired with four different sensors: TerraSAR-X (TSX), and the COSMO-SkyMed constellation (CSK1, CSK2, CSK4), using several different configurations (dual polarization, and two incidence angles: 26° and 36°). Table 1 summarizes the main characteristics of the SAR images recorded at the Kairouan site. All of the images were acquired in the form of "Single Look Complex" products, with the TSX images produced in the Single Look Slant Range Complex (SSC) representation, and the CSK images produced in the Single Look Complex Slant product Balanced (SCS_B) representation. Seven TSX datasets were acquired with Spotlight dual-polarization (HH and VV) at a high incidence angle (36°) and with a ground pixel spacing of approximately 2 m. In the case of the CSK data, four images were acquired in Ping Pong mode using the horizontal and cross polarizations (*HH* and *HV*), at two incidence angles (26° and 36°), with a pixel spacing of approximately 8 m. The SAR images were firstly multi-looked to reduce speckle using the NEST software (available at: https://earth.esa.int/web/nest/home/). When multi-looking is required in the case of CSK images, we consider 2 looks in azimuth and range direction (leading to a resolution of ~ 16 × 16 m^2), whereas in the case of TSX images, 5 looks are used in azimuth and range direction (resulting pixel size ~ 9 × 9 m^2). The images were then radio-metrically calibrated to derive the backscattering coefficients σ^0, and finally geo-referenced using the SRTM 3Sec as a DEM (Auto download in NEST software). The mean radar signals were computed for each training plot.

Table 1. Main characteristics of the X-band SAR images: Pol: Polarization, Inc: Incidence Angle, Desc: Descendant and Asc: Ascendant.

Nr	Sensor	Date of Acquisition (dd/mm/yyyy)	Acquisition Time (UTC)	Acquisition Mode	Pol Mode	Inci.	Orbit	Geometric Resolution (m)
1	CSK1	06/11/2013	17:21:24	PingPong	HV/HH	26°	Desc	7.9
2	TSX	09/11/2013	17:13:34	Spotlight	HH/VV	36°	Asc	1.8
3	TSX	20/11/2013	17:13:34	Spotlight	HH/VV	36°	Asc	1.8
4	CSK1	22/11/2013	17:21:19	PingPong	HV/HH	26°	Desc	7.9
5	TSX	01/12/2013	17:14:17	Spotlight	HH/VV	36°	Asc	1.8
6	CSK4	04/12/2013	17:21:14	PingPong	HV/HH	26°	Desc	7.9
7	CSK2	05/12/2013	17:15:13	PingPong	HV/HH	36°	Desc	7.9
8	TSX	12/12/2013	17:14:17	Spotlight	HH/VV	36°	Asc	1.8
9	TSX	23/12/2013	17:14:16	Spotlight	HH/VV	36°	Asc	1.8
10	TSX	14/01/2014	17:14:15	Spotlight	HH/VV	36°	Asc	1.8
11	TSX	25/01/2014	17:14:15	Spotlight	HH/VV	36°	Asc	1.8

2.2.2. Ground Measurements

Between November 2013 and January 2014, ground campaigns were carried out at the same time as the eleven satellite acquisitions. Fifteen bare soil reference fields were considered with different types of roughness, ranging from smooth to ploughed surfaces (Figure 2). The surface areas of these study

fields ranged between 1.6 ha and 17 ha. The ground measurements made on the test fields involved the characterization of the following soil parameters: soil moisture using a theta-probe instrument, gravimetric sampling, soil roughness using a pin profiler, soil bulk density and soil texture.

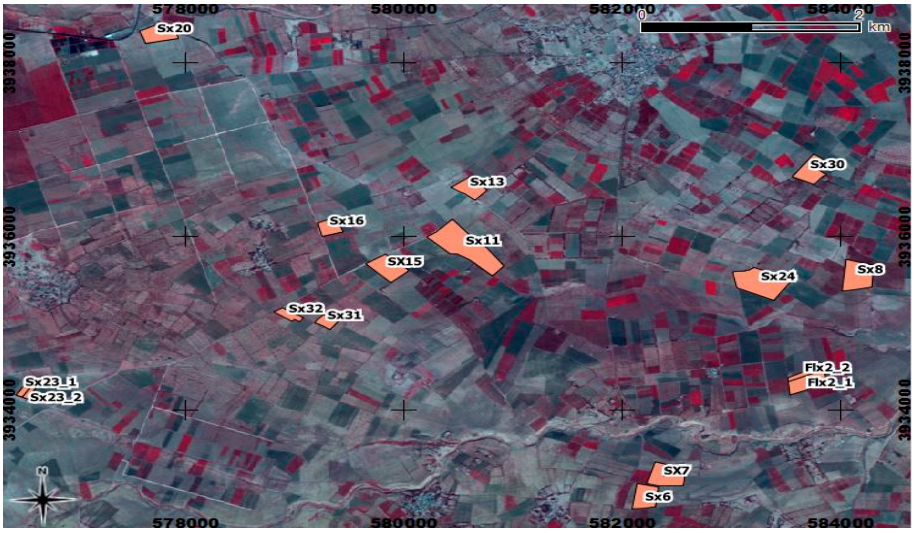

Figure 2. Location of reference fields on the study site (SPOT image).

Soil Moisture

For each training field, approximately ten different gravimetric samples were taken (at depths ranging between 0 and 2 cm), and approximately 20 handheld thetaprobe measurements were made at a depth of 5 cm. These two different depths were used in order to assess the influence of radar penetration depth, which is less than 2 cm at X-band frequencies. The samples were taken from various locations in each reference field, within a two-hour time frame between 15:40 and 17:40, coinciding with the time of each satellite acquisition. The thetaprobe measurements were calibrated with gravimetric measurements recorded during previous campaigns [9].

The gravimetric soil moisture content was computed from the ratio of the mass of water to the mass of dry soil, and was then converted to the volumetric soil moisture using the soil's bulk density (six samples per field). Strong temporal variations in soil moisture content were observed during the experimental campaigns. The volumetric moisture ranged between 4.7% and 31.6% for the thetaprobe measurements, and between 1.2% and 40% for the gravimetric estimations.

Figure 3 illustrates the daily values of precipitation and mean volumetric surface soil moisture, estimated by calculating the mean value of the continuous recordings given by two thetaprobe measurements at a depth of 5 cm. A strong correlation was observed between the soil moisture estimations and precipitation events. Following a precipitation event we generally observe a peak followed by a strong decrease in soil moisture caused the high level of ambient evaporation.

Soil Roughness

Roughness is a measure of micro-topographic height variations at the soil's surface. This was characterized by means of a 1 m long pin profiler with a resolution equal to 2 cm. Ten roughness profiles, 5 parallel and 5 perpendicular to the tillage row direction, were established in all reference

fields during three different ground campaigns. Two main surface roughness parameters, the root mean square surface height (*Hrms*) and the correlation length (*l*), were determined from the mean correlation function, which was computed from the digitized soil profiles [3,10]. Significant variations in the values of *Hrms* were observed between successive ground campaigns, ranging from 0.24 cm (very smooth soils) to 3.4 cm (ploughed soils), resulting mainly from the influence of rain and cultural practices (tillage, sowing…).

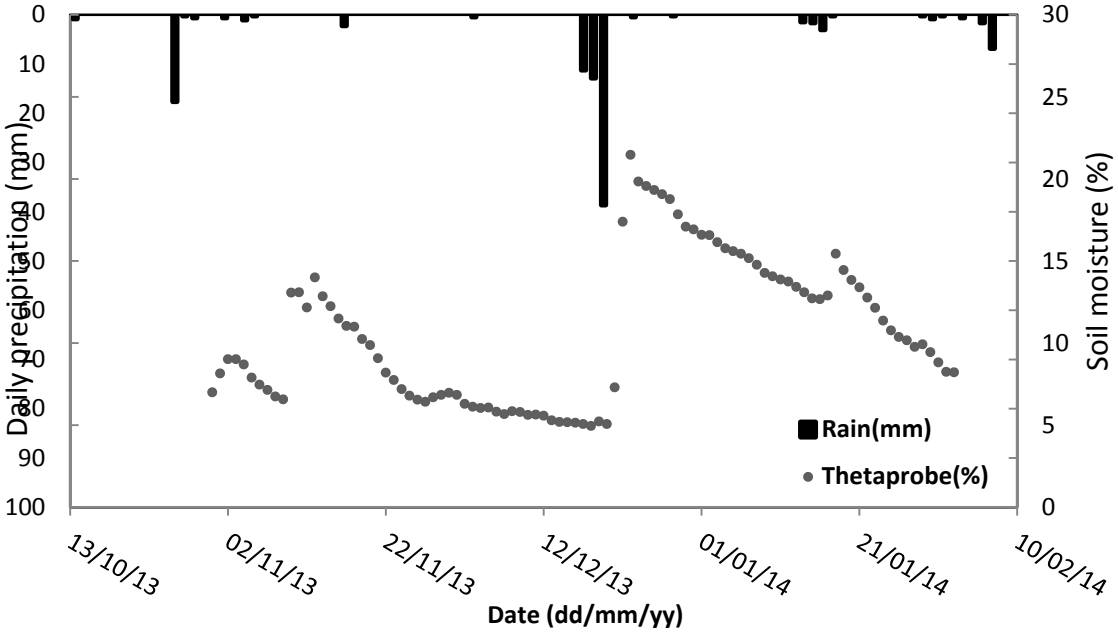

Figure 3. Daily precipitation data and surface soil moisture variations, recorded during the ground campaign with a thetaprobe at 0–5 cm depth.

Soil Texture

For each reference field, three soil samples were collected in order to characterize the soil texture. Various measurements were made in the laboratory to calculate the percentages of sand, silt and clay particles, thus determining the soil's texture. The clay percentages ranged between 18.1% and 47.7% and the sand percentages ranged between 9.95% and 68.8%.

3. Statistical Analysis of Radar Measurements

In this section, we present the results of our statistical analysis of radar measurements as a function of the soil parameters: volumetric soil moisture, and three roughness parameters (*Hrms*, *Zs* and *Zg*), for all of the reference fields.

3.1. Inter-Comparison between TerraSAR-X and COSMO-SkyMed Measurements

In the last two years, several studies making use of TSX and CSK data have revealed the need to inter-calibrate the raw measurement data [38,39], before it is applied to parametric analysis of the soil. Recently, Baghdadi *et al.* [38] compared TSX and CSK signal levels recorded over forests. Although

they observed a temporally stable signal for each of the studied X-band sensors (TSX, CSK1, CSK2, CSK3, CSK4), significant differences reaching approximately 3 dB in the HH polarization and 5 dB in the HV polarization were found in the absolute signal levels measured by these sensors. The results of the comparative analysis established by Pettinato *et al.* [39] have also demonstrated strong differences, equivalent to 4.8 dB, between the signals measured by TSX and CSK2.

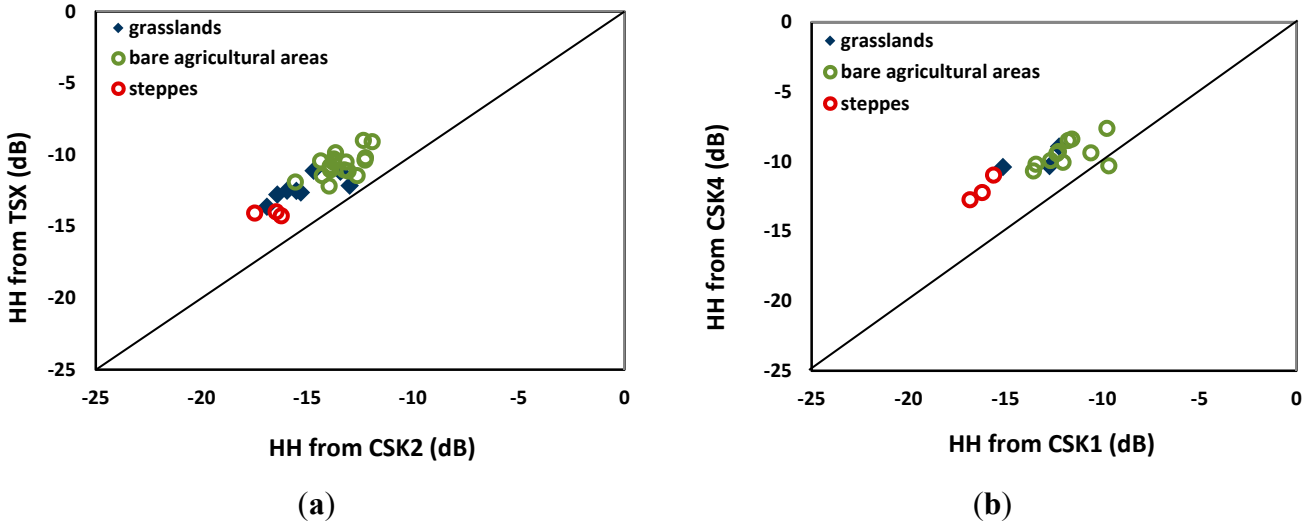

Figure 4. Inter-comparison between COSMO-SkyMed and TerraSAR-X data at *HH* polarization: (**a**) TSX and CSK2 at 36° and (**b**) CSK1 and CSK4 at 26°. Each point corresponds to one homogenous region of Interest.

In the present study, TSX and CSK measurements are compared and analyzed using a large number of targets. Comparisons were established between various pairs of images (TSX and CSK), acquired at the same polarizations and incidence angles. Images recorded at approximately the same date were selected, thus ensuring the presence of similar conditions of soil moisture and roughness. Different large, stable plots (*i.e.*, having just one type of land use: bare agricultural areas, steppes, grasslands, *etc.* were selected, and their mean radar signals were calculated. The mean radar signals in the TSX and CSK2 images recorded at 36° incidence, and in the CSK1 and CSK4 images recorded at 26° incidence, are compared in Figure 4a,b, showing that there are significant differences between the datasets recorded by these pairs of sensors. The mean difference between the TSX and CSK2 images is approximately 2.8 dB, and that between the CSK1 and CSK4 images is approximately 2.9 dB. It is important to note that at 26° incidence, the radar images were acquired in the same descending orbit, whereas at 36° incidence the TSX images were acquired in an ascending orbit and the CSK data was acquired in a descending orbit. Our analysis is based on the observation of targets, some of which are characterized by a limited directional effect. In this context, Zribi *et al.* [40] have shown that in the case of bare soils observed at high incidence angles and high frequencies, the radar signals have a low sensitivity to the azimuth angle. As proposed in Baghdadi *et al.* [38], the signals recorded by TSX and CSK4 were taken as references, such that the CSK2 signals recorded at 36° were corrected by the mean difference (between the TSX and CSK2 images) of 2.8 dB, and the CSK1 signals recorded at 26° were corrected by the mean difference (between the CSK4 and CSK1 images) of 2.9 dB.

3.2. Relationship between Radar Signal and Soil Roughness

In order to analyze the influence of soil roughness on the radar signals, the sensitivity of the TSX and inter-calibrated CSK backscattering coefficients was studied as a function of three different roughness parameters: (i) the root mean surface height *Hrms*; (ii) the parameter $Zs = Hrms^2/l$ [31], and (iii) the parameter $Zg = Hrms(Hrms/l)^{\alpha}$ [32]. This analysis was made in the HH and VV polarizations, at incidence angles equal to 36° and 26°. Figure 5 shows the results corresponding to the HH polarization. In order to extract the influence of roughness only, the data was sorted into two sets: (i) data corresponding to soil with a low volumetric moisture content (less than 10%); and (ii) data corresponding to soil with a high volumetric moisture content (greater than 25%). As no high-moisture images were recorded at low incidence (26°), datapoints corresponding to low soil moisture only are plotted.

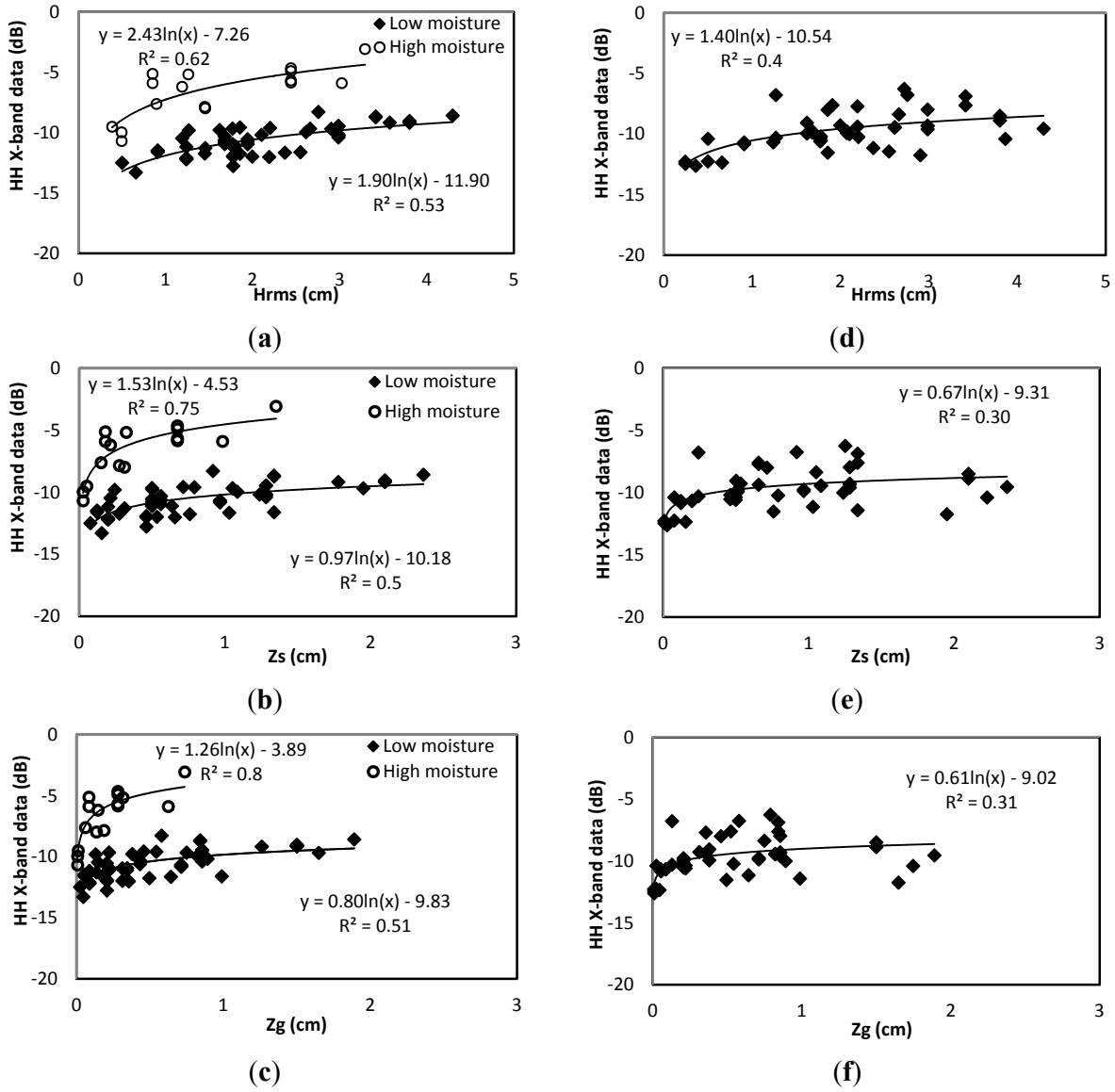

Figure 5. Relationship between X-band SAR signals in the *HH* polarization and the soil roughness parameters *Hrms*, *Zs*, and *Zg*. The data was recorded at 36° incidence, for low and high values of soil moisture (**a**–**c**), and at 26° incidence, for low moisture values only (no high moisture at 26° incidence acquisition dates) (**d**–**f**).

The results show that the radar signals are highly sensitive to all roughness parameters (*Hrms*, *Zs* and *Zg*), at high incidence angles. These relationships are well described by a function in which the radar backscattering coefficient increases linearly with the logarithm of the relevant roughness parameter. This behavior was also observed in several other studies (e.g., [10–12]). The highest correlations are observed with the high moisture set (Figure 5a–c). This could be explained by the presence of high values of surface roughness in the case of low soil moisture only, for which the radar signal nearly reaches saturation. For the high moisture, high incidence (36°) dataset, the radar signals are more strongly correlated with *Zs* (R^2 = 0.75, *p*-value = 0.002) and *Zg* (R^2 = 0.8, *p*-value = 0.002) than with *Hrms* (R^2=0.62, *p*-value=0.001). This behavior is in agreement with the results observed in [32]. The parameter *Zs* combines the influence of both *Hrms* and the soil's roughness correlation length. In addition, it introduces the influence of slope (*Hrms*/*l*), which is an important soil feature in the estimation of σ^0, as shown by [31]. The strongest correlation found with *Zg* can be explained by the fact that it represents the combined influences on radar backscattering of *Hrms*, *l* and the correlation function shape. At a low angle of incidence (θ = 26°), the results shown in Figure 5d–f show that the radar signal is less sensitive to soil roughness than at high incidence, as has been shown by various experimental and theoretical studies [12]. Table 2 summarizes the correlation coefficients of the logarithmic regressions determined for the radar measurements, expressed as a function of soil roughness, for all of the radar configurations. It can be seen that the *VV* and *HH* polarizations lead to approximately similar correlation coefficients.

Table 2. Correlation coefficients retrieved from logarithmic regressions, for various roughness parameters and multi-configuration radar datasets.

		***HH* Polarization**		**VV Polarization**	
		Low Moisture	**High Moisture**	**Low Moisture**	**High Moisture**
36°	*Hrms*	0.53	0.62	0.57	0.6
	Zs	0.5	0.75	0.52	0.77
	Zg	0.51	0.8	0.53	0.8
26°	*Hrms*	0.4			
	Zs	0.3			
	Zg	0.31			

3.3. Relationship between Radar Signal and Soil Moisture Content

Figure 6 shows the behavior of the *HH* polarization signals as a function of volumetric soil moisture derived from thetaprobe measurements (Figure 6a,b), and as a function of gravimetric measurements (Figure 7c,d). Linear relationships are observed between the backscattering coefficients and the volumetric soil moisture at 36° and 26° incidence. These behaviors are observed in several studies as [4,7].

In the case of the data recorded at 36°, the thetaprobe measurements (0–5 cm) are found to be more sensitive (0.26 dB/vol%) than the gravimetric measurements (0.21 dB/vol%). These results can be explained by the fact that the 0–2 cm layer of soil is relatively thin, is more strongly influenced by extremely high and low moisture conditions, and is affected by a larger range of soil moisture values. In practice, the storage capacity of the thin surface layer is quickly saturated during a strong precipitation event. In addition, the upper surface layer is the most strongly affected by evaporation,

under very dry conditions. In the case of the data acquired at 26°, the radar signal is also found to have a good sensitivity to volumetric soil moisture, corresponding to 0.16 dB/vol% for gravimetric sampling and 0.2 dB/vol% for the thetaprobe measurements. It should be noted that due to the relatively restricted range of soil moistures occurring at the time of the low incidence radar acquisitions, weaker correlations are observed at 26° than at 36° incidence. These results are also confirmed in the *VV* polarization (36° incidence), with sensitivity equal to 0.25 dB/vol% for the thetaprobe, and 0.2 dB/vol% for the gravimetric measurements.

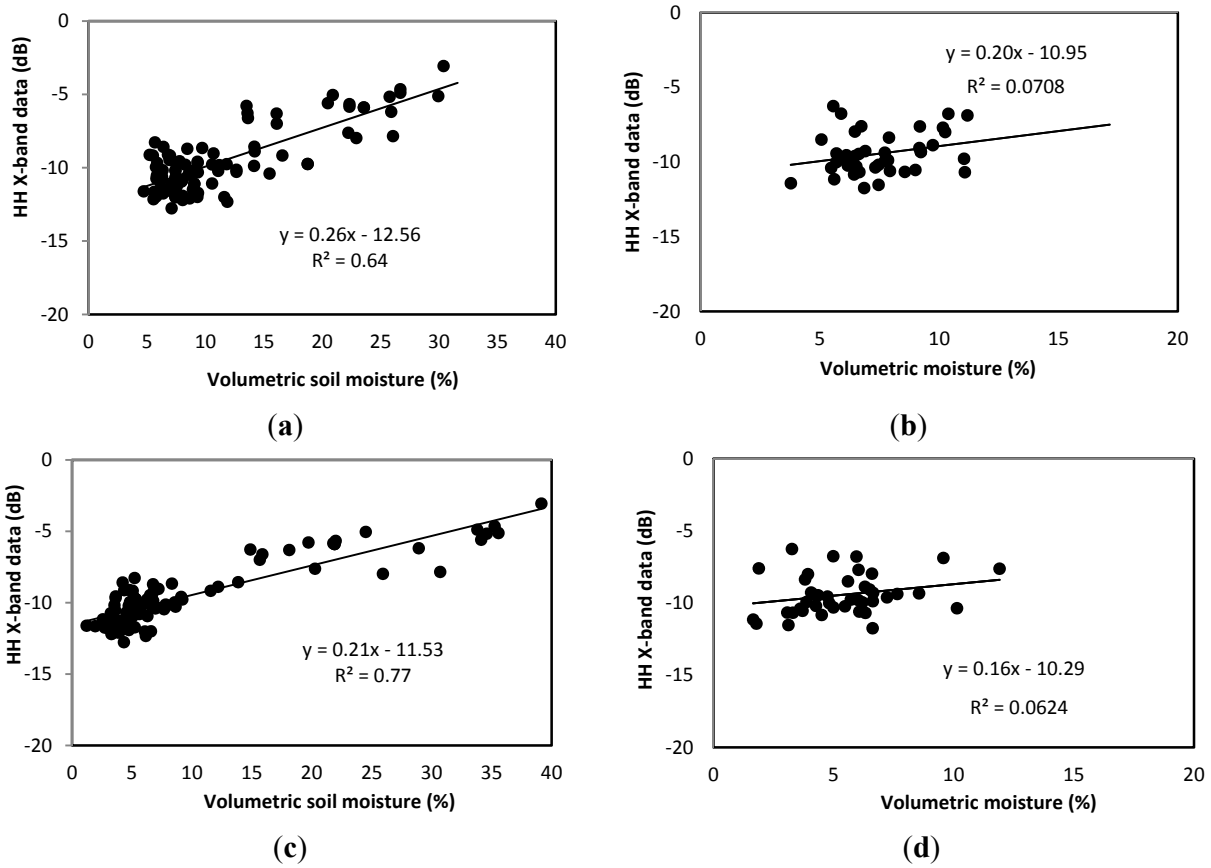

Figure 6. Relationships between backscattering coefficient and measured volumetric soil moisture in the *HH* polarization: (**a**,**b**) for moisture measured with a thetaprobe instrument at a depth of 5 cm, at 36° and 26° incidence; (**c**,**d**) for moisture measured by gravimetric sampling at a depth of 2 cm, at 36° and 26° incidence.

3.4. Relationship between Radar Signal and Soil Parameters

In the previous two sections, we implemented separate analyses of the radar signal's sensitivity to surface roughness and soil moisture. From these results, we propose a simple empirical expression relating the radar signal to these two parameters, *i.e.*, *Mv* (soil moisture) and *Zg* (surface roughness):

$$\sigma_0 = \alpha\, Mv + \beta \log(Zg) + \gamma \quad (1)$$

As the soil moisture is characterized by a small dynamic range at 26° incidence, our analysis was restricted to that of images acquired at 36° incidence. Our radar data was divided into two datasets: the first of these was used to estimate the parameters of the empirical model, and the second was used for

its validation. The coefficients α, β and γ were fitted using the least squares method. For the *HH* polarization, α = 0.22, β = 0.85 and γ = −11.14, with R^2 = 0.82. For the *VV* polarization, the following values were found: α = 0.20, β = 0.59 and γ = −11.21, with R^2 = 0.82. Figure 7 shows a plot comparing the values computed using this empirical relationship with those recorded in the second experimental dataset. The agreement between experimental radar data and simulated values is found to be excellent, with an RMS error of 1 dB in the *HH* polarization, and 0.94 dB in the *VV* polarization.

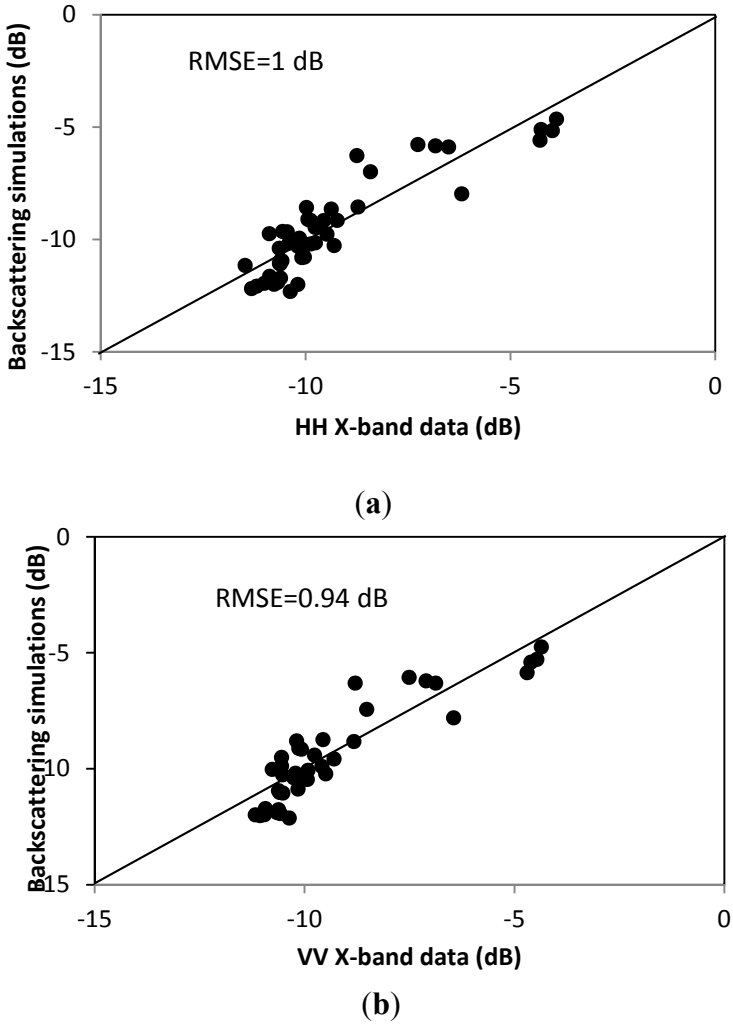

Figure 7. Validation of the empirical model used to simulate radar signal strength at 36° incidence, as a function of soil moisture and soil roughness: (**a**) *HH* polarization; (**b**) *VV* polarization.

4. Evaluation of Backscattering Models

In this section, we evaluate the accuracy of various backscattering models: IEM model; Dubois model; and the Baghdadi-calibrated IEM model, by comparing the predicted signal strengths with the remotely sensed radar data. *In situ* measurements from our database (soil moisture and surface roughness) were used to provide input to the models. The discrepancies observed between the real and simulated signals are expressed in the form of two statistical indices: root mean square error (RMSE) and bias.

4.1. IEM Model

The Integral Equation Model is a physical radar backscattering model, developed by Fung and Chen [13]. For bare agricultural soils, it simulates the σ^0_{HH}, σ^0_{HV} and σ^0_{VV} radar backscattering coefficients as a function of various radar configurations and soil parameters. The IEM's domain of applicability covers a wide range of roughness values [13], which can be approximated by $k \times Hrms < 3$, corresponding to $Hrms < 1.5$ cm in the X-Band, where k is the wavenumber of the radar signal. Two types of surface correlation function, exponential or Gaussian, are used in the IEM backscatter model simulations. The exponential correlation function is generally used to represent smooth natural surfaces, whereas the Gaussian function is used to describe high surface roughness values [41]. Figures 8 and 9 compare the IEM model with measured radar data, at 36° incidence (*HH* and *VV* polarizations) and at 26° incidence (*HH* polarization).

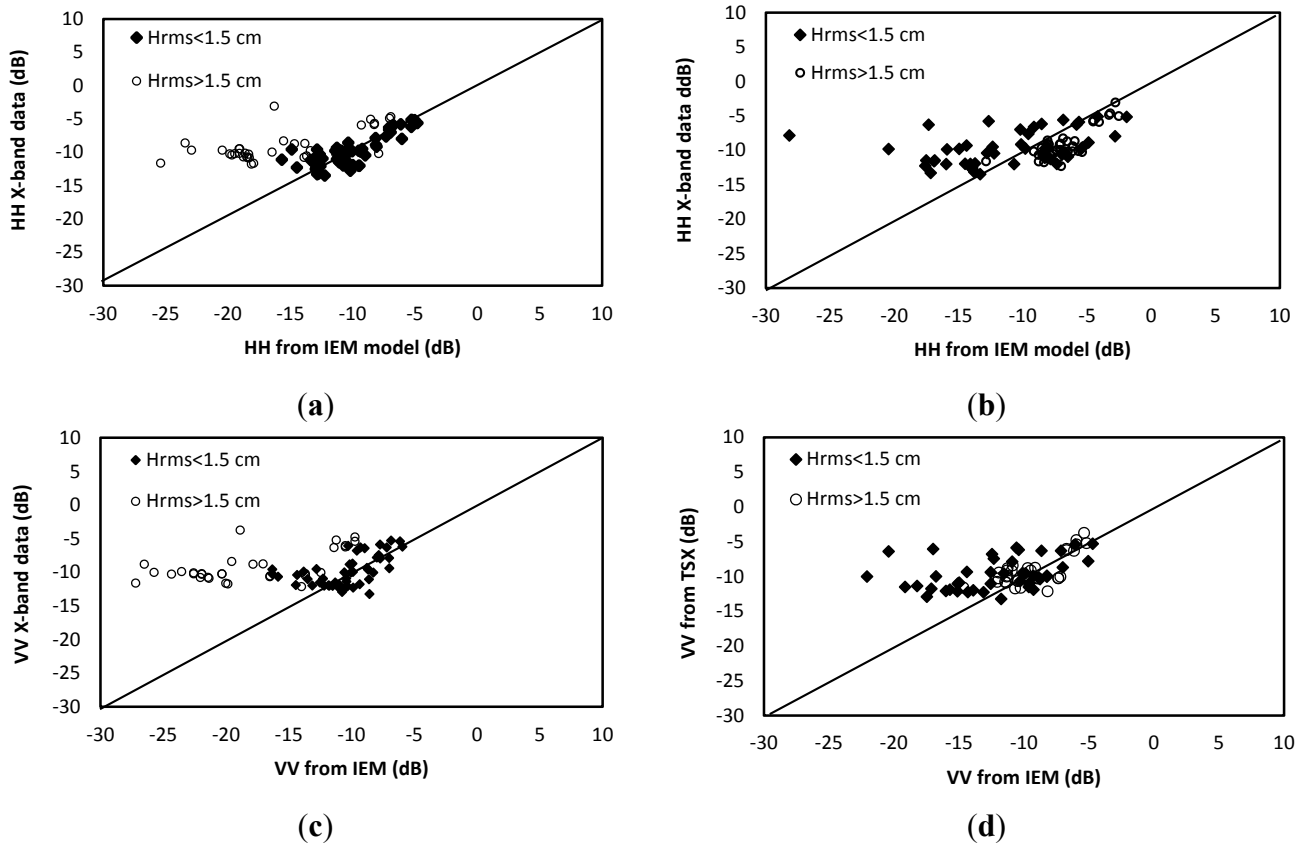

Figure 8. Comparison between measured X-band data and IEM simulations, at 36° incidence: *HH* polarization: (**a**) exponential correlation function and (**b**) Gaussian correlation function; *VV* polarization: (**c**) exponential correlation function and (**d**) Gaussian correlation function.

The results show that the IEM simulations are in good agreement with the remotely sensed signals under certain conditions only:

- In the *HH* polarization, for $Hrms < 1.5$ cm, with an exponential correlation function: at $\theta = 36°$, bias = 0.29 dB and RMSE = 1.59 dB; and at $\theta = 26°$, bias = 0.08 dB and RMSE = 3.54 dB. On

the other hand, the IEM model tends to over-estimate the backscattering coefficient σ^0_{HH} in the following cases: *Hrms* > 1.5 cm with a Gaussian correlation function: bias approximately −2.31 and −1.98 dB, and RMSE equal to 2.64 and 2.9 dB, for θ = 36° and θ = 26°, respectively.

- In the *VV* polarization, for *Hrms* < 1.5 cm, with an exponential correlation function: at θ = 36°, bias = 0.63 dB and RMSE = 2.4 dB. For *Hrms* > 1.5 cm, with a Gaussian correlation function: at 36°, bias = 0.24 and RMSE = 1.66 dB.

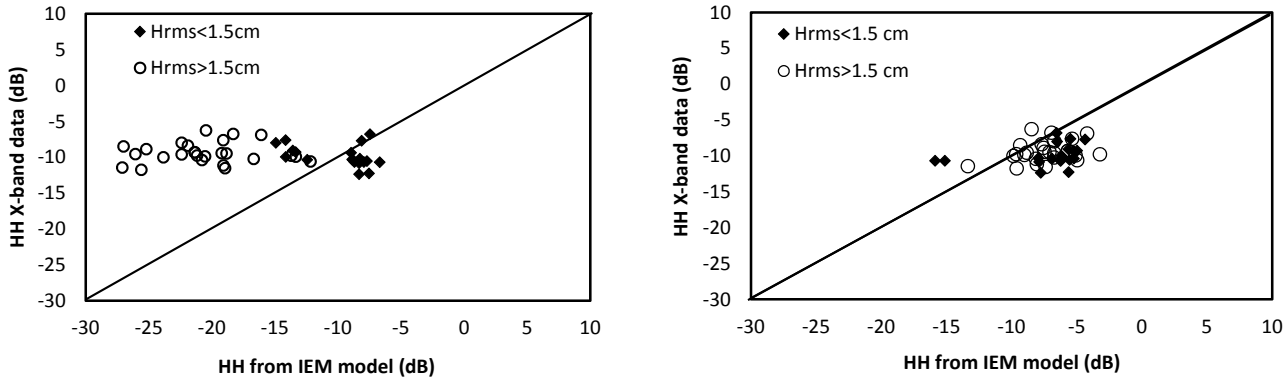

Figure 9. Comparison between measured X-band data and IEM simulations at 26° incidence in the *HH* polarization: (**a**) exponential correlation surface; (**b**) Gaussian correlation function.

Using X-band data and various incidence angles in the range between 25° and 52°, Baghdadi *et al.*, [30] observed that the IEM correctly simulates the values of σ^0_{HH} and σ^0_{VV} for the following two cases: *Hrms* < 1.5 cm with an exponential correlation function; and *Hrms* >1.5 cm with a Gaussian function.

4.2. Dubois Model

The Dubois model is a semi empirical backscattering model, developed by Dubois *et al.* [18]. It simulates the σ^0_{HH} and σ^0_{VV} radar backscatter coefficients using as input the incidence angle (θ°), the dielectric constant, the *Hrms* surface height, and the radar wavelength. Figure 10 shows that this model is in good agreement with the measured σ^0_{VV} data, only for the case where *Hrms* > 1.5 cm and θ = 36°, with a corresponding bias of −0.18 dB and RMSE of 1.75 dB. The Dubois model often tends to over-estimate the SAR backscattering coefficients at θ = 36° when *Hrms* > 1.5 cm, with a bias of approximately −2.6 dB and an RMSE of 3.4 dB, and at θ = 26° for all values of Hrms, with a bias of approximately −4.6 dB and an RMSE of 5.5 dB. On the other hand, at θ = 36° this model underestimates the radar signal in the case of low surface roughness (*Hrms* < 1.5 cm), with a bias of approximately 2.32 dB and an RMSE of 3.25 dB in the *HH* polarization, and a bias of approximately 3.5 dB and an RMSE of 3.9 dB in the *VV* polarization.

4.3. Baghdadi Calibrated IEM Version

In the following paragraph, the semi-empirical calibration of the IEM model developed by Baghdadi *et al.* [33–36] is applied, in order to minimize the mismatch between the IEM simulations and the observed backscattered signal. In this new version of the IEM, the measured correlation length

is replaced by a fitting parameter "Lopt", whatever the range of Hrms. The use of Lopt has been tested under various SAR configurations, in the X and C bands, and at both HH and VV polarizations [33–36]. The results show firstly that the implementation of Lopt leads to an improved agreement between the IEM simulations and the SAR data. Secondly, it also allows the IEM's domain of validity to be extended, to include even high values of surface roughness (Table 3). Finally, it makes it possible to restrict the use of roughness parameters to that of Hrms only. This is very useful for the inversion of data, using a generally small number of radar configurations. These modifications are proposed for the Gaussian correlation function shape, which leads to the best agreement between simulations and data, when the new fitting parameter Lopt is used.

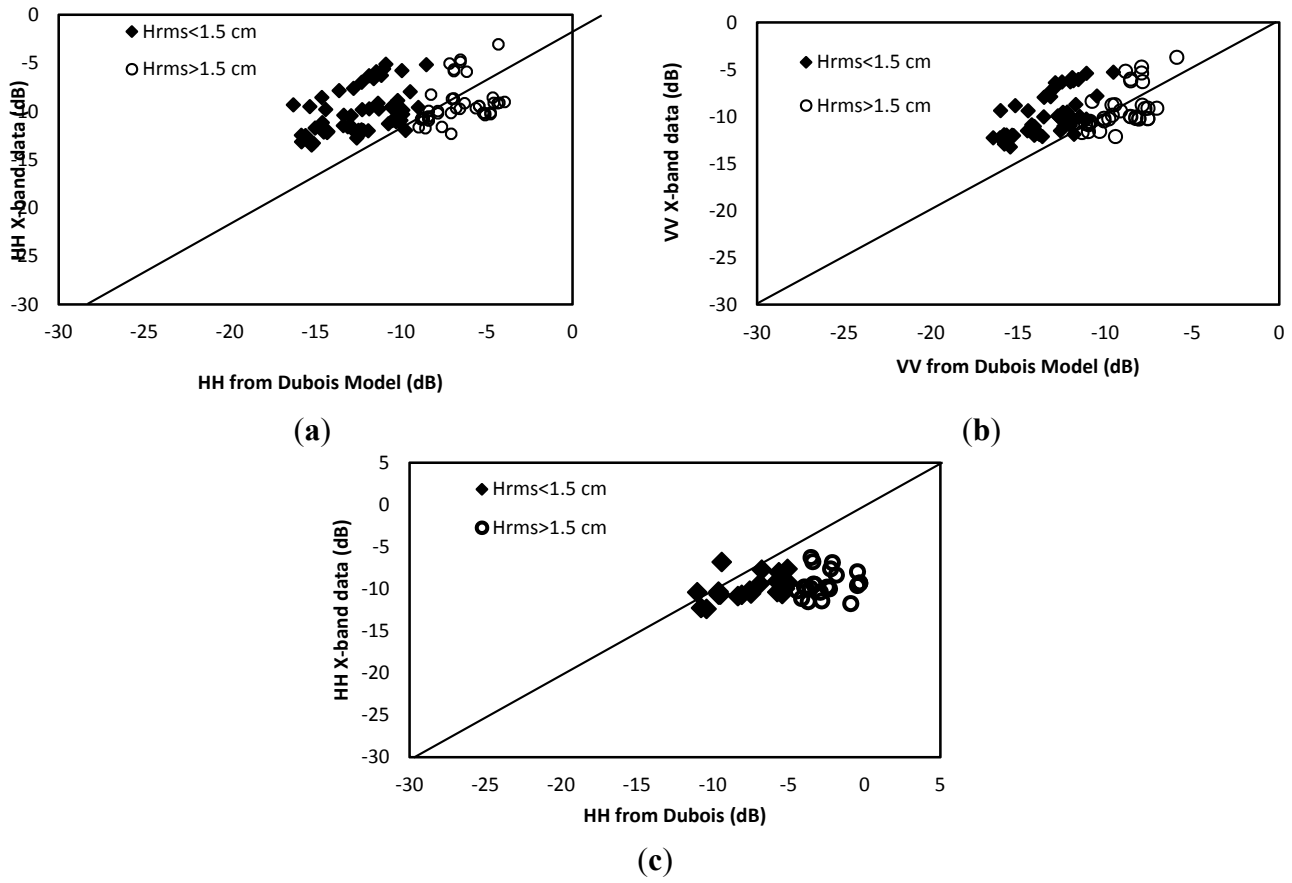

Figure 10. Comparison between X-band data and Dubois simulations: (**a**) *HH* polarization, at 36° incidence; (**b**) *VV* polarization, at 36° incidence; (**c**) *HH* polarization, at 26° incidence.

In the X-band, when the Gaussian correlation function is used, Lopt is written as [36]:

$$Lopt\left(Hrms,\theta,HH\right)=18.102\,e^{-0.033\theta}Hrms^{0.7644\,e^{0.0035\theta}}\text{, for HH polarization} \quad (2)$$

$$Lopt\left(Hrms,\theta,VV\right)=18.075\,e^{-0.0379\theta}Hrms^{1.2594\,e^{-0.0145\theta}}\text{, for VV polarization} \quad (3)$$

where θ is expressed in degrees, and Lopt and *Hrms* are expressed in centimeters.

Figure 11 compares the measured radar data with simulated signals obtained with the initial version (using the measured correlation length), and with the empirical calibrated version (using the fitting parameter Lopt) of the IEM model. In these two versions, σ^0_{HH} and σ^0_{VV} are computed using the Gaussian correlation function.

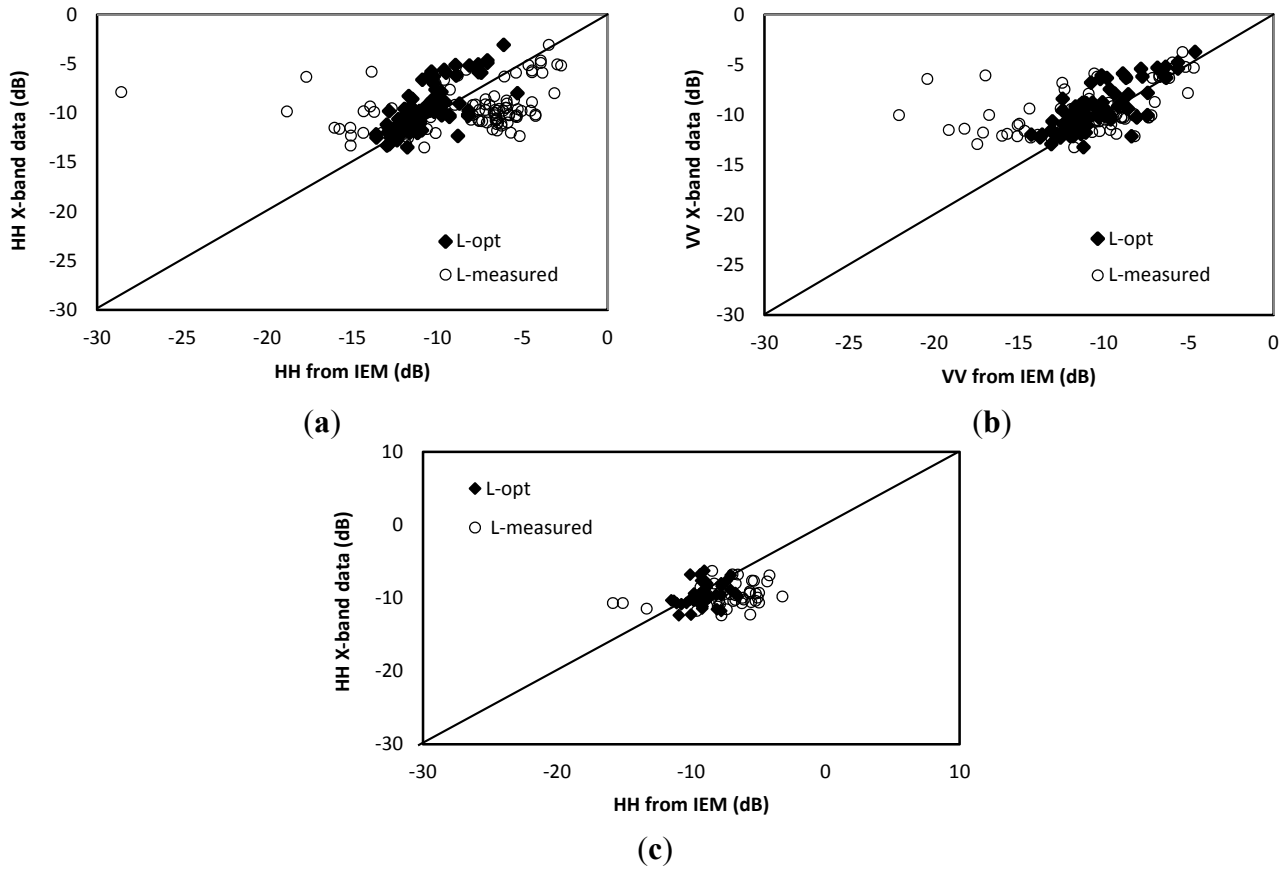

Figure 11. Comparison between X-band radar signals and Baghdadi-calibrated IEM [36] simulations: (**a**) *HH* polarization; 36° incidence angle; (**b**) *VV* polarization, 36° incidence; (**c**) *HH* polarization, 26° incidence.

Table 3. Main statistical indexes (Bias and RMSE) for the IEM model, Dubois model, and the IEM model calibrated using Lopt, described by Baghdadi *et al.* [36], in the *HH* and *VV* polarizations.

		HH Polarization		**VV Polarization**	
IEM Model (Using Measured Correlation Length)					
		Bias (dB)	**RMSE (dB)**	**Bias (dB)**	**RMSE (dB)**
36° (Exponential function)	*Hrms* < 1.5 cm	0.29	1.59	0.63	2.41
	Hrms > 1.5 cm	4.56	7.78	6.04	9.21
	All *Hrms*	2.11	5.2	3.34	6.72
36° (Gaussian function)	*Hrms* < 1.5 cm	3.42	8.2	4.32	8.36
	Hrms > 1.5 cm	−2.31	2.64	0.24	1.66
	All *Hrms*	0.99	6.5	3	6.9
26° (Exponential function)	*Hrms* < 1.5 cm	0.08	3.54		
	Hrms > 1.5 cm	11.1	11.8		
	All *Hrms*	6.45	3.05		
26° (Gaussian function)	*Hrms* < 1.5 cm	−1.28	3.6		
	Hrms > 1.5 cm	−1.98	2.89		
	All *Hrms*	−1.2	3		

Table 3. *Cont.*

		HH Polarization		VV Polarization	
		Dubois Model			
		Bias (dB)	**RMSE (dB)**	**Bias (dB)**	**RMSE (dB)**
36°	*Hrms* < 1.5 cm	2.32	3.25	3.48	3.9
	Hrms > 1.5 cm	−2.57	3.38	-0.18	1.75
	All *Hrms*	0.22	3.3	1.91	1.78
26°	*Hrms* < 1.5 cm	−2.19	2.85		
	Hrms > 1.5 cm	−6.8	7.08		
	All *Hrms*	−4.6	5.49		
IEM calibrated Model according to Baghdadi *et al.* [36]					
36° (all *Hrms*)		0.97	1.8	0.84	1.67
26° (all *Hrms*)		−0.55	1.64		

In the HH polarization, the results predicted by the semi-empirical IEM calibration are found to be in good agreement with the measured backscatter coefficients, with a bias of approximately −0.5 and 0.9 dB, and an RMSE of approximately 1.64 and 1.8 dB, at 26° and 36°, respectively. In the VV polarization, at 36°, the bias (difference between the IEM simulations, using Lopt and σ^0_{TSX}) is 0.84 dB and the RMSE is equal to 1.67 dB. Application of the initial version of the IEM (using the measured correlation length and a Gaussian correlation function) leads to considerable discrepancies, with an RMSE of 6.5 and 3 dB in the HH polarization, at 36° and 26° respectively, and an RMSE of approximately 6.9 dB in the VV polarization, at 36°.

The results determined using the semi-empirical calibration are in good agreement with those obtained in [36], and lead to a significant improvement in the IEM backscattering predictions. The calibrated IEM approach thus provides a robust model for the simulation of radar backscattering from agricultural soils.

5. Conclusions

In this study, the sensitivity of X-band SAR signals to physical soil parameters is analyzed for the case of bare agricultural soils. Remotely sensed data, recorded by two SAR systems (the TSK and CSK constellations) over a semi-arid region in Tunisia, is compared with *in situ* measurements of soil moisture and surface roughness. The first step in this process involves the inter-calibration of four different X-band sensors (TSX, CSK1, CSK2, CSK4). As reported in other studies, strong offsets are observed between the signals measured by these sensors. An empirical calibration of the CSK1 and CSK2 signals is proposed, in which the latter are referenced to the signals recorded by the TSK and CSK4 sensors, respectively. Logarithmic relationships are then observed between the multi-configuration backscattering coefficients extracted from the TSX and CSK sensor data and the surface roughness parameters: *Hrms* (root mean square height), *Zs* and *Zg*. The strongest correlation (R^2 = 0.8) is obtained with the parameter *Zg*, at 36° incidence. This can be explained by the fact that *Zg* combines the influence of several conventional roughness parameters (*Hrms*, correlation length and correlation function shape). A linear correlation is observed between the radar signals and the measured values of volumetric soil moisture, at angles of incidence equal to 26° and 36°. The strongest sensitivities are

obtained from the thetaprobe moisture measurements made at 0–5 cm. An empirical model is proposed to simulate radar signals as a function of soil moisture and the surface roughness parameter *Zg*. Validation of the proposed expressions with a second dataset reveals an excellent agreement between measurements and simulations, with an RMS error equal to 1 dB and 0.94 dB for the *HH* and *VV* polarizations, respectively.

The performance of the IEM, Dubois, and Baghdadi-calibrated IEM [36] models are also discussed. In practice, the IEM model correctly simulates the response of X-band radar sensors under the following conditions: Hrms < 1.5 cm, use of an exponential correlation function, HH polarization at 26° and 36° incidence; Hrms < 1.5 cm, use of an exponential correlation function, VV polarization; Hrms > 1.5 cm, use of a Gaussian function, both polarisations at 36° incidence. Significant discrepancies (over- or underestimations) are generally observed between the measured X-band SAR signals and the backscattering predicted by the Dubois model. Considerable improvements are observed in the performance of the IEM model when the IEM Baghdadi-calibrated version is implemented, with for example (between measured and simulated radar signals): biases of approximately −0.5 and 0.9 dB, and RMSE's of approximately 1.64 and 1.8 dB, in the HH polarization, at 26° and 36° incidence, respectively.

The results presented in this paper confirm the usefulness of X-band SAR (*HH* and *VV*) data for the retrieval and mapping of soil properties near the surface over bare agricultural soils. In future studies, the present authors will apply X-band SAR data to this type of analysis.

Acknowledgments

This study was funded by MISTRALS/SICMED, the ANR AMETHYST *(ANR-12 TMED-0006-01*) and TOSCA/CNES projects. Procurement of the CSK images used in this analysis was supported by public funds received in the framework of GEOSUD, a project (*ANR-10-EQPX-20*) of the "Investissements d'Avenir" (Investments for the Future) program managed by the French National Research Agency. We also wish to thank all of the technical teams of the IRD and INAT (Institut National Agronomique de Tunisie) for their strong collaboration and support in implementing the ground-truth measurements.

Author Contributions

Azza Gorrab: Ground measurements and data analysis;
Mehrez Zribi: Data analysis and results interpretation;
Nicolas Baghdadi: Results interpretation;
Bernard Mougenot: Ground measurements;
Zohra Lili-Chabaane: Participation to experimental campaigns organization.

Conflicts of Interest

The authors declare no conflict of interest.

References

1. Ulaby, F.T.; Moore, R.K.; Fung, A.K. *Microwave Remote Sensing Active and Passive*; Artech House, Inc.: Norwood, MA, USA, 1986.
2. Koster, R.D.; Dirmeyer, P.A.; Guo, Z.; Bonan, G.; Chan, E.; Cox, P.; Gordon, C.T.; Kanae, S.; Kowalczyk, E.; Lawrence, D.; *et al.* Regions of strong coupling between soil moisture and precipitation. *Science* **2004**, *305*, 1138–1140.
3. Jackson, T.-J.; Schmugge, J.; Engman, E.-T. Remote sensing applications to hydrology: Soil moisture. *Hydrol. Sci.* **1996**, *41*, 517–530.
4. Moran, M.S.; Hymer, D.C.; Qi, J.; Sano, E.E. Soil moisture evaluation using multi-temporal synthetic aperture radar (SAR) in semiarid rangeland. *Agric. For. Meteorol*. **2000**, *105*, 69–80.
5. Zribi, M.; Saux-Picart, S.; André, C.; Descroix, L.; Ottlé, O.; Kallel, A. Soil moisture mapping based on ARSAR/ENVISAT radar data over a sahelian site. *Int. J. Remote Sens*. **2006**, *28*, 3547–3565.
6. Marticorena, B.; Kardous, M.; Bergametti, G.; Callot, Y.; Chazette, P.; Khatteli, H.; Le Hégarat-Mascle, S.; Maillé, M.; Rajot, J.L.; Vidal Madjar, D.; *et al.* Geometric and aerodynamic surface roughness in southern Tunisia and their relation with radar backscatter coefficient. *J. Geophys. Res.* **2006**, doi:10.1029/2006JF000462.
7. Paloscia, S.; Pampaloni, P.; Pettinato, S.; Santi, E. A comparison of algorithms for retrieving soil moisture from ENVISAT/ASAR images. *IEEE Trans. Geosci. Remote Sens.* **2008**, *46*, 3274–3284.
8. Rahman, M.M.; Moran, M.S.; Thoma, D.P.; Bryant, R.; Holifield Collins, C.D.; Jackson, T.; Orr, B.J.; Tischler, M. Mapping surface roughness and soil moisture using multi-angle radar imagery without ancillary data. *Remote Sens. Environ.* **2008**, *112*, 391–402.
9. Zribi, M.; Chahbi, A.; Lili Chabaane, Z.; Duchemin, B.; Baghdadi, N.; Amri, R.; Chehbouni, A. Soil surface moisture estimation over a semi-arid region using ENVISAT ASAR radar data for soil evaporation evaluation. *Hydrol. Earth Syst. Sci*. **2011**, *15*, 345–358.
10. Baghdadi, N.; Zribi M.; Loumagne, C.; Ansart, P.; Anguela, T.P. Analysis of TerraSAR-X data and their sensitivity to soil surface parameters over bare agricultural fields. *Remote Sens. Environ*. **2008**, *112*, 4370–4379.
11. Aubert, M.; Baghdadi, N.; Zribi, M.; Douaoui, A.; Loumagne, C.; Baup, F.; El Hajj, M.; Garrigues S. Analysis of TerraSAR-X data sensitivity to bare soil moisture, roughness, composition and soil crust. *Remote Sens. Environ*. **2011**, *115*, 1801–1810.
12. Anguela, T.P.; Zribi, M.; Baghdadi, N.; Loumagne, C. Analysis of local variation of soil surface parameters with TerraSAR-X radar data over bare agricultural fields. *IEEE Trans. Geosci. Remote Sens.* **2010**, *48*, 874–881.
13. Fung, A.K.; Li, Z.; Chen, K.S. Backscattering from a randomly rough dielectric surface. *IEEE Trans. Geosci. Remote Sens*. **1992**, *30*, 356–369.
14. Fung, A.K. *Microwave Scattering and Emission Models and Their Applications*; Artech House: Boston, MA, USA, 1994.
15. Chen, K.S.; Wu, T.D.; Tsang, L.; Li, Q.; Shi, J.; Fung, A.K. Emission of rough surfaces calculated by the integral equation method with comparison to three-dimensional moment method simulations. *IEEE Trans. Geosci. Remote Sens*. **2003**, *41*, 90–101.

16. Wu, T.D.; Chen, K.S. A reappraisal of the validity of the IEM model for backscattering from rough surfaces. *IEEE Trans. Geosci. Remote Sens*. **2004**, *42*, 743–753.
17. Oh, Y.; Sarabandi, K.; Ulaby, F.T. An empirical model and an inversion technique for radar scattering from bare soil surfaces. *IEEE Trans. Geosci. Remote Sens*. **1992**, *30*, 370–382.
18. Dubois, P.; Van Zyl, J.; Engman, T. Measuring soil moisture with imaging radars. *IEEE Trans. Geosci. Remote Sens*. **1995**, *33*, 915–926.
19. Wu, T.D.; Chen, K.S.; Shi, J.; Fung, A.K. A transition model for the reflection coefficient in surface scattering. *IEEE Trans. Geosci. Remote Sens*. **2001**, *39*, 2040–2050.
20. Li, Q.; Shi, J.C.; Chen, K.S. A generalised power law spectrum and its applications to the backscattering of soil surfaces based on the integral equation model. *IEEE Trans. Geosci. Remote Sens*. **2002**, *40*, 271–281.
21. Le Morvan, A.; Zribi, M.; Baghdadi, N.; Chanzy, A. Soil moisture profile effect on radar signal measurement. *Sensors* **2008**, *8*, 256–270.
22. Shi, J.; Wang, J.; Hsu, A.Y.; O'Neill, P.E.; Engman, E.T. Estimation of bare surface soil moisture surface roughness parameter using L-band SAR image data. *IEEE Trans. Geosci. Remote Sens*. **1997**, *35*, 1254–1265.
23. Mattia, F.; Le Toan, T. Backscattering properties of multi-scale rough surfaces. *J. Electro. Waves Appl.* **1999**, *13*, 491–526.
24. Davidson, M.W.; Le Toan, T.; Mattia, F.; Satalino, G.; Manninen, T.; Borgeaud, M. On the characterization of agricultural soil roughness for radar remote sensing studies. *IEEE Trans. Geosci. Remote Sens.* **2000**, *38*, 630–640.
25. Mattia, F.; Davidson, M.W.J.; Le Toan, T.; D'Haese, C.M.F.; Verhoest, N.E.C; Gatti, A.M.; Borgeaud, M. A Comparison between soil roughness statistics used in surface scattering models derived from mechanical and laser profilers. *IEEE Trans. Geosci. Remote Sens.* **2003**, *41*, 1659–1671.
26. Zribi, M.; Ciarletti, V.; Taconet, O. Validation of a rough surface model based on fractional brownian geometry with SIRC and ERASME radar data over Orgeval site. *Remote Sens. Environ*. **2000**, *73*, 65–72.
27. Callens, M.; Verhoest, N.E.C.; Davidson, M.W.J. Parameterization of tillage-induced single-scale soil roughness from 4-m profiles. *IEEE Trans. Geosci. Remote Sens.* **2006**, *44*, 878–888.
28. Verhoest, N.E.C.; Lievens, H.; Wagner, W.; Alvarez-Mozos, J.; Moran, M.S.; Mattia, F. On the soil roughness parameterization problem in soil moisture retrieval of bare surfaces from Synthetic Aperture Radar. *Sensors* **2008**, *8*, 4213–4248.
29. Lievens, H.; Vernieuwe, H.; Alvarez-Mozos, J.; de Baets, B.; Verhoest, N.E.C. Error in SAR-derived soil moisture due to roughness parameterization: An analysis based on synthetical surface profiles. *Sensors* **2009**, *9*, 1067–1093.
30. Lievens, H.; Verhoest, N.E.C.; de Keyser, E.; Vernieuwe, H.; Matgen, P. Álvarez-Mozos J.; de Baets, B. Effective roughness modelling as a tool for soil moisture retrieval from C- and L-band SAR. *Hydrol. Earth Syst. Sci*. **2011**, *15*, 151–162.
31. Zribi, M.; Dechambre, M. A new empirical model to retrieve soil moisture and roughness from radar data. *Remote Sens. Environ*. **2003**, *84*, 42–52.
32. Zribi, M.; Gorrab, A.; Baghdadi, N. A new soil roughness parameter for the modelling of radar backscattering over bare soil. *Remote Sens. Environ*. **2014**, *152*, 62–73.

33. Baghdadi, N.; Gherboudj, I.; Zribi; M.; Sahebi, M.; Bonn, F.; King, C. Semi-empirical calibration of the IEM backscattering model using radar images and moisture and roughness field measurements. *Int. J. Remote Sens.* **2004**, *25*, 3593–3623.
34. Baghdadi, N.; Holah, N.; Zribi M. Calibration of the integral equation model for SAR data in C-band and HH and VV polarizations. *Int. J. Remote Sens.* **2006**, *27*, 805–816.
35. Baghdadi, N.; Abou Chaaya, J.; Zribi, M. Semi-empirical calibration of the integral quation model for SAR data in C-band and cross polarization using radar images and field measurements. *IEEE Geosci. Remote Sens. Lett.* **2011**, *8*, 14–18.
36. Baghdadi, N.; Saba, E.; Aubert, M.; Zribi, M.; Baup, F. Evaluation of radar backscattering models IEM, Oh, and Dubois for SAR data in X-band over bare soils. *IEEE Geosci. Remote Sens. Lett*. **2011**, *8*, 1160–1164.
37. Macelloni, G.; Paloscia, S.; Pampaloni, P.; Sigismondi, S.; de Matthaeis, P.; Ferrazzoli, P.; Schiavon, G.; Solimini, D. The SIR-C/X-SAR experiment on Montespertoli: Sensitivity to hydrological parameters. *Int. J. Remote Sens*. **1999**, *20*, 2597–2612.
38. Baghdadi, N.; El Hajj, M.; Dubois, P.; Zribi, M.; Belaud, G.; Cheviron, B. Signal level comparison between TerraSAR-X and COSMO-SkyMed SAR sensors. *IEEE Geosci. Remote Sens. Lett.* **2015**, *12*, 448–452.
39. Pettinato, S.; Santi, E.; Paloscia, S.; Pampaloni, P.; Fontanelli, G. The intercomparison of X-band SAR images from COSMO-SkyMed and TerraSAR-X satellites: Case studies. *Remote Sens.* **2013**, *5*, 2928–2942.
40. Zribi, M.; Ciarletti, V.; Taconet, O.; Vidal-Madjar, D. Effect of rows structure on radar microwave measurements over soil surface. *Int. J. Remote Sens*. **2002**, *23*, 5211–5224.
41. Zribi, M.; Baghdadi, N.; Holah, N.; Fafin, O.; Guérin, C. Evaluation of a rough soil surface description with ASAR-ENVISAT Radar Data. *Remote Sens. Environ*. **2005**, *95*, 67–76.